Published in final edited form as:
Nat Struct Mol Biol. 2006 November ; 13(11): 987–995. doi:10.1038/nsmb1164.

Three-dimensional structure of the KChIP1–Kv4.3 T1 complex reveals a cross-shaped octamer

Marta Pioletti[1,3], **Felix Findeisen**[1,3], **Greg L Hura**[2], and **Daniel L Minor Jr**[1]

[1]Cardiovascular Research Institute, Departments of Biochemistry and Biophysics and Cellular and Molecular Pharmacology, California Institute for Quantitative Biomedical Research, University of California, San Francisco, California 94143-2532, USA.

[2]Lawrence Berkeley National Laboratory, University of California, Berkeley, California 94720, USA.

Abstract

Brain I_A and cardiac I_{to} currents arise from complexes containing Kv4 voltage-gated potassium channels and cytoplasmic calcium-sensor proteins (KChIPs). Here, we present X-ray crystallographic and small-angle X-ray scattering data that show that the KChIP1–Kv4.3 N-terminal cytoplasmic domain complex is a cross-shaped octamer bearing two principal interaction sites. Site 1 comprises interactions between a unique Kv4 channel N-terminal hydrophobic segment and a hydrophobic pocket formed by displacement of the KChIP H10 helix. Site 2 comprises interactions between a T1 assembly domain loop and the KChIP H2 helix. Functional and biochemical studies indicate that site 1 influences channel trafficking, whereas site 2 affects channel gating, and that calcium binding is intimately linked to KChIP folding and complex formation. Together, the data resolve how Kv4 channels and KChIPs interact and provide a framework for understanding how KChIPs modulate Kv4 function.

In biological systems, electrical information is encoded and processed by changes in action-potential timing, duration, frequency, waveform and number[1]. Modulation of voltage-gated potassium channels is central to these events and affects heart rate, sensory transduction and cognition. The ion transport[2] and voltage-dependent gating properties[3] of the potassium channel α subunits that form the ion conduction pathway are well characterized. Although α subunits form the pore, many channels function as complexes that require cytoplasmic and transmembrane auxiliary subunits[4]. To date, little is known regarding the way in which such components bind α subunits and modulate channel action. Understanding the interplay between regulatory components and pore-forming domains is crucial for unraveling how modulatory signals[4] and homeostatic mechanisms[5] allow excitable cells to sense and respond to environmental cues.

Two potassium currents, I_A (ref. [6]) and I_{to} (ref. [7]), exert strong control over neuronal and cardiac excitability, respectively, and provide clear examples of the importance of auxiliary subunits for tuning properties of α subunits. Both currents arise from complexes of Kv4

Correspondence should be addressed to D.L.M. (daniel.minor@ucsf.edu)..
[3]These authors contributed equally to this work.

Accession codes. Protein Data Bank: Coordinates and structure factors have been deposited with accession code 2I2R.

Note: Supplementary information is available on the Nature Structural & Molecular Biology website.

COMPETING INTERESTS STATEMENT
The authors declare that they have no competing financial interests.

voltage-gated potassium channel subunits with a family of soluble calcium-sensor 'Kv-channel interacting proteins', KChIPs[6,8–10]. A related protein, frequenin, has effects on Kv4s that are similar to those of KChIPs[10,11]. KChIPs and frequenin belong to the large family of neuronal calcium-sensor proteins[8,12]. Although the presence of calcium-sensor proteins as essential components of the I_A and I_{to} complexes suggests that calcium may be important for channel regulation, no clear physiological demonstration of this link has been given.

KChIPs have profound effects on the properties of Kv4 α subunits. Their coexpression with Kv4s increases current density, changes channel inactivation kinetics and speeds recovery from inactivation[8,13–16]. The KChIP-Kv4 interaction requires the Kv4 N-terminal cytoplasmic domain, which comprises a ~40-residue N-terminal hydrophobic segment that is unique to Kv4 channels[8,13,15], and the Kv channel assembly domain, T1 (ref. [17]). KChIP–Kv4 complexes have deep evolutionary roots. Genes for each member are found in chordates as primitive as *Ciona intestinalis*[18]. Cell-biological studies suggest that interactions between KChIPs and the N-terminal hydrophobic segment regulate channel trafficking to the plasma membrane[13,15,19]. Loss of KChIP2 function leads to enhanced arrhythmia susceptibility, underscoring the crucial nature of the KChIP-Kv4 interaction[20].

The way KChIPs and Kv4 channels associate remains unresolved. Three studies have suggested mutually exclusive models. Biochemical work has shown that, in addition to interactions with the N-terminal hydrophobic segment that precedes the T1 domain, KChIP interactions with a loop on the T1 cytoplasmic face, the 'docking loop', are important[17]. These data led to the suggestion that KChIPs dock underneath the T1 complex in a way that resembles the Kv1 T1 domain–Kvβ subunit interaction, where two tetrameric structures dock in series[21]. In contrast, an interpretation of low-resolution (21 Å) negative-stain images of complete KChIP2–Kv4.2 complexes has suggested a model where the KChIPs are not underneath the T1 domains but rather form a square-shaped planar structure in which the KChIPs run parallel to the T1 tetramer sides[22]. The third model originates from studies of an engineered KChIP1 in which the first 30 residues of the Kv4.2 hydrophobic N terminus were fused directly to the C-terminal end of the final KChIP1 helix, H10. The chimera formed dimers in solution. From these data, the authors concluded that KChIP dimers associate with the T1 domain in a way that breaks with the four-fold symmetry of the α subunit[23].

Here, we report crystallographic and solution experiments that demonstrate that the KChIP1–Kv4.3 T1 complex is a cross-shaped octamer with four-fold rotational symmetry that matches the pore-forming domains[21]. The structure resolves the question of how these proteins interact and defines two sites of KChIP-Kv4 interactions that have distinct functional roles in channel trafficking and gating.

RESULTS

The KChIP1–Kv4.3 N-terminal cytoplasmic domain complex

We used a coexpression strategy to define which lengths and combinations of Kv4 N-terminal cytoplasmic domains and KChIP isoforms formed soluble, well-behaved complexes in *Escherichia coli*. We crystallized a complex of the rat Kv4.3 (also called Kcnd3) N-terminal cytoplasmic domain (residues 1–143) and human KChIP1 (also called KCNIP1; residues 37–216) containing the conserved, functional KChIP core[24]. Initial crystals diffracted poorly and could not be improved. Thus, we used surface entropy reduction and converted selected surface lysine residues to alanine[25]. A double mutant (K160A K167A) in the nonconserved KChIP1 EF3-EF4 linker yielded crystals that diffracted X-rays to 3.35 Å. Electrophysiological examination showed that KChIP1(K160A

K167A)–Kv4.3 channel complexes were indistinguishable from wild-type complexes (data not shown).

The structure of the KChIP1–Kv4.3 T1 complex shows that the assembly forms a cross-shaped octamer having the T1 tetramer at the center (Fig. 1a, chains A–D) and individual KChIPs extending radially (Fig. 1a, chains E–H). The asymmetric unit has two octameric complexes that are apposed on the cytoplasmic T1 faces (Fig. 1b). T1 shows few differences from the isolated Kv4.3 T1 structure[17] (r.m.s. deviation = 0.64 Å^2 over 408 Cα positions). In contrast, KChIP1 shows substantial differences (r.m.s. deviation = 4.03 Å^2 over 179 Cα positions) from isolated KChIP1 (ref. [17]).

The structure reveals two main interaction sites. Site 1 buries ~2,100 Å^2 total surface area between residues 3 and 21 of a conserved hydrophobic segment that is on the N-terminal side of T1 (called T1N; Fig. 2a) and a large hydrophobic pocket (28 Å long, 12 Å deep, 10 Å wide) formed by KChIP1 (Fig. 2b,c). T1N contains residues essential for KChIP-Kv4 interaction[8,13] and has two parts: an α-helix, residues 4–17 (the T1N helix), and a loop, residues 18–39, lacking regular secondary structure (the T1N linker). Site 2 comprises contacts between the KChIP1 H2 helix and the T1 domain docking loop that bury ~900 Å^2 (Fig. 2d). Each KChIP1 uses site 1 interactions to bind T1N from one Kv4.3 monomer but makes site 2 interactions with the adjacent T1 monomer (Fig. 1a). The contacts with two T1 subunits seen in this arrangement are consistent with the report that, in full-length channels, KChIP binding can overcome T1 assembly defects[26] and may endow the KChIP–Kv4 T1 complex with cooperative properties that affect gating.

As in other KChIP structures[17,23], only EF3 and EF4 of the EF-hand calcium-binding loop sequences are in the calcium-bound state (Fig. 2e and Supplementary Fig. 1 online). EF1 lacks key calcium-binding residues and is empty. EF2 is unoccupied and is distorted by the binding of the T1N helix (Supplementary Fig. 1).

KChIP1–Kv4.3 T1 site 1 interactions

Comparison with the isolated KChIP1 structure[17] indicates that a large conformational change creates site 1. The H10 helix moves to the rim of the wide, hydrophobic groove (Fig. 2e). This conformation is comparable to the frequenin structure (Supplementary Fig. 1), where the hydrophobic pocket is occupied by polyethylene glycol molecules from the crystallization solution[27]. The similar conformational change suggests that H10 displacement from its position as a cover over the site 1 hydrophobic pocket is a general mechanism by which KChIPs and frequenin bind target proteins.

The T1N helix interacts with the KChIP1 hydrophobic pocket in a parallel orientation. This orientation is opposite to that observed in a fusion protein in which the first 30 N-terminal residues of Kv4.2 are fused covalently to the KChIP1 H10 helix C terminus[23], where the identical Kv4.2 T1N residues do not induce a conformational change in the site 1 pocket (Supplementary Fig. 1). Three observations support our T1N register and orientation assignment. First, we observed strong electron density for T1N Trp8, Phe11 and Trp19 (Supplementary Fig. 2 online). Second, T1N residues 21–39 have sufficiently clear density in noncrystallographic symmetry–averaged maps to define the T1N connectivity with T1 (Supplementary Fig. 2). Third, the Sed atom of Met20 (Supplementary Fig. 2) has clear density (4.5 σ) at the expected position in noncrystallographic symmetry–averaged anomalous difference maps generated using the amplitudes from a crystal of the selenomethionine (SeMet)-substituted complex. These results unambiguously support our assigned helix direction and register and suggest that the previously reported structure is a consequence of the unnatural fusion.

T1N residues 7–21, which are strongly conserved (Fig. 2a), make most of the interactions with the KChIP1 hydrophobic pocket. The three aromatic residues, Trp8, Phe11 and Trp19, each of which is important for KChIP-Kv4 interaction and current modulation[23,28], fit into hydrophobic crevices within the site 1 pocket (Fig. 2c). Trp8 contacts KChIP1 Phe60, Val69, Phe74, Ile77 and Phe111. Phe11 contacts an adjacent crevice composed of KChIP1 Phe98, Phe111, Ala114, Leu115, Leu118 and Trp129. Trp19 interacts with KChIP1 Tyr134, Ile150, Ile154 and Tyr155 as well as T1N Met20. The short stretch of conserved T1N alanines (Ala12, Ala14, Ala15 and Ala16; Fig. 2a) allow the T1N helix to fit tightly into the KChIP1 pocket.

The contacts between T1N and KChIP1 are concordant with previous studies. Deletion analyses have shown that truncation of Kv4.2 residues 2–20 (ref. [13]), and the shorter truncation of residues 7–11, but not 2–6 (ref. [17]), greatly reduce interactions of KChIP with the Kv4.2 cytoplasmic N-terminal domain. Furthermore, identification by lysine scanning mutagenesis of Ile17, Gly18 and Met20 as residues crucial for interaction[28] also fits well with the intimate interaction of these positions with the hydrophobic pocket.

KChIP1–Kv4.3 T1 site 2 interactions

Site 2 buries 900 Å^2 in an interface of mixed hydrophilic and hydrophobic character in which the KChIP1 H2 helix contacts the α2 T1 helix and the docking loop on the cytoplasmic face of the T1 complex (Fig. 2d). Kv4.3 Phe73 contributes the major hydrophobic component and is involved in aromatic stacking interactions with KChIP1 Tyr57. The Kv4.3 Asp78 side chain is positioned to form a salt bridge with KChIP1 Arg51. The Kv4.3 Glu72 and Phe75 main chain oxygens appear within hydrogen-bonding distance of KChIP1 Gln54. Finally, the Kv4.3 Glu70 side chain is well situated to contact the side chains of KChIP1 Tyr57 and Lys61. Kv4.3 T1 docking loop residues Glu70, Phe73 and Asp78, which are identical to residues in Kv4.2 known to be crucial for KChIP-Kv4.2 interactions[17,28], reside squarely in the site 2 interface and support the relevance of the structure with respect to the full-length channel.

Small angle X-ray scattering analysis of the complex

We used small-angle X-ray scattering (SAXS)[29] to probe the KChIP1$_{37–216}$–Kv4.3$_{1–143}$ complex structure in solution and test whether the flat, cruciform octamer is the preferred arrangement or a consequence of crystallization. SAXS provides an independent assessment of the overall shape of protein molecular envelopes at ~10- to 20-Å resolution[29].

Two different analyses, the Guinier approximation and GNOM[30], yielded similar values for the radius of gyration (R_g = 42.8 ± 0.7 Å and 43.5 ± 0.4 Å, respectively). The scattering element distribution described by the $P(r)$ function defines the longest axis in the complex (D_{max} = 155 ± 5 Å; Supplementary Fig. 3 online). These R_g and D_{max} values agree with those calculated by CRYSOL[31] for our crystal structure of the octamer (R_g = 42.6 Å and D_{max} = 150 ± 5 Å).

We used GASBOR[32] to calculate low-resolution *ab initio* models of three-dimensional arrangements of scattering centers that reproduce the SAXS data and provide the shape of the molecular envelope of the complex (Supplementary Fig. 3). Because this inverse scattering problem has no unique solution, we performed ten independent runs for three different symmetries (*P*1, *P*2 and *P*4) and compared and averaged the models from each using DAMAVER[33]. Calculations using *P*1 or *P*2 symmetry showed wide variations in the distributions of dummy residues that did not converge. In contrast, the models obtained using *P*4 symmetry converged and fit experimental scattering data well (χ^2 = 3.46). The resulting model is cross-shaped (Supplementary Fig. 3) and strongly resembles our

crystallographically determined complex. Comparison of the calculated scattering profile from our crystallographic structure using CRYSOL[31] and the measured data shows excellent agreement (χ^2 = 3.03) that is also evident from superposition of the octamer structure and SAXS model (Fig. 3a).

A flat, four-fold symmetric arrangement of the KChIP–Kv4 T1 complex has been proposed from low-resolution (21 Å) negative-stain images of KChIP2–Kv4.2 (ref. [22]). Superposition of a square-shaped complex similar to that proposed in ref. [22], in which the KChIPs run laterally to the T1 domains, shows poor overlap with the SAXS model (Fig. 3b). This square-shaped arrangement has an inferior correlation to the SAXS data, compared with the crystallographic cross-shaped octamer, when the scattering curves are compared using CRYSOL (χ^2 = 7.06) and has substantially smaller R_g and D_{max} values (R_g = 36.1 Å, D_{max} = 110 ± 5 Å) than the experimental values (see above). These great differences exclude the possibility that there is an appreciable population of the square-shaped arrangement in solution, eliminate the possibility that the cross-shaped character of the *ab initio* SAXS model results solely from the use of *P*4 symmetry and provide a noteworthy example of the power of SAXS to vet competing models of macromolecular complex architecture. Furthermore, dynamic light-scattering experiments, as well as comparison of the expected SAXS profiles of the individual components and the unit cell hexadecameric arrangement, firmly support the conclusion that the complex is an octamer (Supplementary Fig. 3). Together, these data show that the shape of complex has not been forced by crystallization conditions and strongly suggest that the cruciform complex reflects the native KChIP1–Kv4.3 arrangement.

Separate roles of sites 1 and 2 in trafficking and gating

Because the structure defines a previously uncharacterized KChIP-T1 interface, site 2, we mutated key KChIP1 residues in this interface (Arg51, Gln54, Tyr57 and Lys61) to alanine to examine its functional role. *Xenopus laevis* oocyte two-electrode voltage clamp experiments revealed that Y57A and K61A mutations did not alter surface expression but clearly perturbed the inactivation kinetics of the channel complex, such that the mutants resembled channels lacking KChIPs (Fig. 4a,b and Table 1). R51A and Q54A perturbed neither gating nor surface expression. The double mutant, Y57A K61A, had inactivation and recovery-from-inactivation properties indistinguishable from Kv4.3 channels lacking KChIPs (Fig. 4b,c and Table 1) yet retained the potent effect on current enhancement (Fig. 4a and Table 1). Consistent with the smaller buried surface area at site 2 compared with site 1, none of the mutations caused substantial perturbation of binding to the HMT-Kv4.3$_{1–143}$ fusion protein (Fig. 4d). Together, these data suggest that site 1 and site 2 have two separate roles. Site 1 interactions seem to be largely responsible for KChIP-Kv4 association and for mediating channel trafficking effects, whereas site 2 interactions influence channel inactivation and recovery from inactivation.

Calcium effects on KChIP conformation and binding

In neuronal calcium-sensor proteins such as KChIPs, calcium-dependent conformational changes of the EF hands are thought to be important for function[12]. Simultaneous disablement of KChIP EF2, EF3 and EF4 eliminates modulation of Kv4 currents[8]. Because the importance of calcium binding to each functional KChIP EF hand was unknown, we mutated the first calcium-coordinating aspartate of each one singly (EF2, D99A; EF3, D135A; EF4, D183A), in pairs (EF2 EF3, D99A D135A; EF2 EF4, D99A D183A; EF3 EF4, D135A D183A) and as a triple mutant (EF2 EF3 EF4, D99A D135A D183A) and tested the mutants' ability to bind the HMT-Kv4.3$_{1–143}$ fusion protein. The single mutants and the EF2 EF3 and EF2 EF4 double mutants did not measurably impair binding. In contrast, the EF3 EF4 and EF2 EF3 EF4 mutants were clearly defective (Fig. 5a).

To understand why certain KChIP1 mutants did not bind, we expressed and purified KChIP1 and each mutant individually to characterize their properties. KChIP1 and the EF2, EF4 and EF2 EF4 mutants each eluted from a gel-filtration column in a single peak corresponding to a monomer (Supplementary Fig. 4 online). In contrast, the EF3 and EF2 EF3 mutants eluted in several peaks corresponding to a mixture of monomer and aggregated protein. Both EF3 EF4 and EF2 EF3 EF4, the mutants that did not bind the intracellular N-terminal Kv4.3 domain, eluted as a peak that had a substantially higher molecular weight than wild-type KChIP1 (Supplementary Fig. 4). SDS-PAGE analysis showed apparently stoichiometric amounts of a protein that we identified by western blotting as the *E. coli* chaperone DnaK (Supplementary Fig. 4). The tight association of these chaperone–KChIP EF-hand mutant complexes suggests that KChIP folding and calcium binding are intimately linked.

We used spectroscopic experiments to characterize further the structural consequences of KChIP-calcium interactions. Circular dichroism experiments show that reduction of free calcium concentration causes KChIP1 to become less helical (Fig. 5b). Dynamic light-scattering experiments indicate that this KChIP1 conformational change is concomitant with the conversion from a well-behaved monodisperse protein into a form that aggregates (Supplementary Fig. 4). We obtained similar results for the EF2, EF4 and EF2 EF4 mutants (data not shown). Together with the biochemical data, these results demonstrate that calcium binding is required for proper KChIP folding and is essential for binding to Kv4 channels.

The observation that EF2 EF3 EF4 binds poorly to the Kv4 N-terminal cytoplasmic domain disagrees with reports using full-length channels[8], where interactions with the Kv4 C-terminal cytoplasmic domain[28] and localization of full-length KChIP1 to the membrane by an N-terminal myristoylation[34] may also contribute. To discover whether these factors may compensate the defects caused by the EF-hand mutations and to gain further insight into the role of calcium, we pursued functional characterization of full-length Kv4.3 with KChIP1 EF-hand mutants in *Xenopus* oocytes. As reported[8], coexpression of Kv4.3 and KChIP1 increases current amplitude, slows inactivation and speeds recovery from inactivation (Table 1). Current amplitudes and kinetic properties of Kv4.3 coexpressed with the EF2, EF4 or EF2 EF4 mutant were similar to those upon coexpression with wild-type KChIP1. The two mutants with poor biochemical properties (EF3 and EF2 EF3) had concentration-dependent effects (Fig. 5c–e). At a 1.5:1 Kv4.3/KChIP1 mRNA molar ratio, EF3 and EF2 EF3 mutants behave similarly to wild-type KChIP1. Reduction in the relative amount of KChIP1 (3.5:1 Kv4.3/KChIP1) spared the effects of wild-type KChIP1 on kinetics but made the EF3 and EF2 EF3 mutants ineffective at modulation. In agreement with their severely impaired binding ability, EF3 EF4 and EF2 EF3 EF4 mutants had no effect on current peak amplitudes or kinetics and produced channels similar to Kv4.3 alone (Fig. 5c–e). Together, these results indicate that KChIP calcium binding is important for Kv4.3 binding and channel modulation.

DISCUSSION

Our work provides the first high-resolution description of KChIP-Kv4 association. The identification of site 1 and site 2 as principal points of contact agrees with previous mutagenesis data that indicated the importance of both the T1N segment[13,17] and the T1 docking loop[17,28]. The planar, cross-shaped octameric structure of the complex clearly differs from the previously suggested structural models[17,22,23] and resolves the question of how KChIPs and Kv4 N-terminal cytoplasmic domains interact. Superposition of the KChIP1–Kv4.3 complex and the homologous Kv1.2 T1 domains in the Kv1.2 channel structure[21] (Fig. 6a) suggests a notable offset between the positions of the KChIPs and the

voltage sensors (Fig. 6b) and a resemblance to the overall shape of the particles seen in KChIP2–Kv4.2 complex[22].

Each Kv4 subunit has a ~150- to 200-residue C-terminal cytoplasmic domain. Topological considerations require that this domain exits the transmembrane domain near the four-fold central axis of the pore and near T1 (ref. [35]), where it may make specific interactions with T1 and the KChIPs. Negative-stain images of KChIP2–Kv4.2 show pillars of density at the complex periphery that could represent part of the α subunit's C-terminal domain[22], and functional studies indicate that C-terminal truncations of the a subunit may interfere with KChIP-Kv4 assembly[28]. Thus, other points of direct KChIP-Kv4 physical interaction may contribute to assembly and gating.

Fast inactivation of Kv4 channels seems to be fundamentally different from the Shaker-type 'ball-and-chain' mechanism, in which the N-terminal cytoplasmic segment of the protein is thought to enter and block the channel pore[1]. Kv4 inactivation is thought to arise from the concerted action of the N- and C-terminal cytoplasmic domains[36]. Although the Kv4 N terminus can influence inactivation in the absence of KChIPs[37,38], the intimate association of T1N and KChIP excludes the possibility that KChIP–Kv4 inactivation occurs by a ball-and-chain mechanism and supports the idea that T1 conformational changes are coupled to Kv channel gating[35,39,40]. Exactly how KChIPs, T1 and the α subunit's transmembrane segments are mechanistically coupled remains to be explained. In light of the primacy of site 2 for modulating inactivation and recovery from inactivation, the interaction of KChIP with more than one T1 subunit offers a likely means by which KChIPs could influence gating.

Different KChIP isoforms affect α-subunit kinetics in distinct ways[41–43]. Most KChIP variability resides in the nonconserved N-terminal region absent from our structure. It seems likely that this KChIP portion is responsible for the varied functional effects[41–43]. A truncated KChIP (KChIP2d) lacking the entire protein except for EF4 has been reported to affect channel properties[16,44]. Because KChIP2d lacks the site 1 hydrophobic cleft and all of site 2, the reported functional effects are unlikely to be related to the function of intact KChIPs.

Kvβ cytoplasmic subunits also bind T1 and affect channel function[21,45–47]. These subunits can bind Kv4s[48,49], and simultaneous overexpression of KChIP2 and Kvβ3 produces channels with unique properties[50]; however, it is unclear whether native Kv4s associate simultaneously with KChIPs and Kvβs. Comparison of KChIP1–Kv4.3 T1 and Kv1.2–Kvβ[21] complexes indicates that the two accessory subunits bind opposite faces of the T1 docking loop and suggests that formation of a Kv4–KChIP–Kvβ complex is possible (Fig. 6c,d). Superposition of T1 in the KChIP–Kv4.3 T1 complex with T1 in the Kvβ–Kv1.2 complex[21] (Fig. 6d) shows remarkably little steric clash between the structures, except for two side chain pairs whose clashes could easily be relieved by rotamer changes. Thus, the T1 docking loop may serve as a site for KChIP–Kv4 channels to engage Kvβ or other modulatory proteins that could further tune channel properties. The potential serial arrangement (Fig. 6c) suggests an organizational principle for ion-channel complex formation: the membrane layer contains the pore and voltage sensors, whereas the membrane-proximal layer contains assembly information and components that regulate gating and trafficking; this membrane-proximal layer may in turn accept input from a distal layer comprising other regulatory cytoplasmic factors.

An important question is whether there is an *in vivo* link between calcium levels and Kv4 function. Cell-biological studies have demonstrated that without KChIPs, Kv4 channels do not reach the plasma membrane efficiently and are largely retained intracellularly[15,51]. Coexpression with KChIP1, KChIP2 or KChIP3 causes a marked redistribution of channels

to the plasma membrane that requires functional EF hands[51]. Our data show that in the absence of calcium, KChIP1 has a strong tendency to unfold and aggregate. Binding to the Kv4 N-terminal cytoplasmic domain and modulation of channels are also impaired. Thus, without calcium, KChIPs are unable to bind and modulate Kv4 channels. These results suggest that intracellular calcium changes could alter the quantity of fully assembled KChIP–Kv4 complexes in the membrane. Whether such regulation is acute (milliseconds to seconds) or on a longer timescale (minutes to hours) remains to be determined. Our demonstration of the importance of calcium for KChIP folding and Kv4 association suggests that the latter may be crucial.

In cardiac ventricles, the I_{to} transmural gradient seems to be determined by KChIP2 expression levels[52,53]. Decreases in I_{to} are associated with cardiac arrhythmias[7,20] and the cardiac action-potential prolongation that is associated with cardiac hypertrophy and heart failure[7,54]. I_A has a nonuniform density distribution in dendrites and is important in action-potential backpropagation[6]. Changes in cardiac I_{to} and neuronal I_A may reflect the ability of Kv4 channel complexes to sense and respond to environmental cues that are a part of normal or pathophysiological processes. In this respect, the link between calcium-mediated folding of KChIPs, binding to Kv4 α subunits and increased surface expression may be important. Furthermore, small molecules that could alter I_{to} or I_A channel activity by modulating KChIP-Kv4 interactions could tune the excitability of a variety of tissues[55]. The KChIP1–Kv4.3 T1 structure provides the necessary molecular architecture for detailed investigation of how persistent changes in calcium levels might affect channel regulation and may prove an important guide in the development of new channel pharmacopeias.

METHODS

Protein expression and purification

Rat Kv4.3$_{1–143}$ (GenBank L48619) was cloned into a modified pET28 vector containing a His$_6$ tag, maltose-binding protein (MBP) and a tobacco etch virus cleavage site on the N terminus of the protein sequence (pET28-HMT)[56]. Human KChIP1 (residues 37–216; IMAGE clone) was cloned into a pEGST vector lacking the glutathione *S*-transferase (GST) tag[57]. Both vectors were cotransformed into *E. coli* BL21(DE3)pLysS. Protein expression and purification details can be found in Supplementary Methods online.

Crystallization and structure determination

Crystals of native KChIP1$_{37–216}$(K160A K167A)–Kv4.3$_{1–143}$ complexes and SeMet-substituted complexes were obtained at room temperature by hanging drop vapor diffusion and flash-frozen in mother liquor supplemented with 20% (v/v) glycerol. Data were collected at Lawrence Berkeley National Laboratories Advanced Light Source (ALS) beamline 8.3.1 (Table 2). Details of the crystallization, structure solution and refinement procedures can be found in Supplementary Methods.

Circular dichroism and dynamic light-scattering analysis

Circular dichroism spectra of KChIP1$_{37–216}$ and EF mutants at 20 μM in 250 mM KCl and 10 mM HEPES (pH 7.4), in the presence of 1 mM Ca^{2+} and 0–10 mM EGTA, were recorded on an Aviv 215 circular dichroism spectrometer using a 1-mm-path-length quartz cell at 20 °C. Dynamic light-scattering experiments used a DynaPro instrument (Wyatt Technologies).

Electrophysiology

Constructs for electrophysiology were subcloned into a pGEMHE derivative[58]. RNA transcripts (Ampliscribe, Epicentre Technology) were injected into *Xenopus* oocytes as

described[58]. Kv4.3 and KChIP1 mRNA final concentrations were 12.5 ng μl^{-1} and 5 ng μl^{-1}, respectively, unless otherwise indicated. Two-electrode voltage-clamp experiments were performed 1 or 2 d after injection using CLAMPLEX 8.2.0.244, previously described protocols[59] and a GeneClamp 500B (Axon Instruments) amplifier controlled by a computer with a 1,200-MHz processor (Celeron, Gateway), and digitized with a Digidata 1332A (Axon Instruments). Recording solutions contained 90 mM NaCl, 2 mM $MgCl_2$ and 10 mM HEPES (pH 7.4), adjusted with NaOH. Data were analyzed using Clampfit (Axon Instruments).

Small angle X-ray scattering

SAXS data were collected at ALS beamline 12.3.1 (Lawrence Berkeley National Laboratory) on protein complexes at 8 mg ml^{-1} and 16 mg ml^{-1}. Details of data collection and data processing can be found in Supplementary Methods.

Supplementary Material

Refer to Web version on PubMed Central for supplementary material.

Acknowledgments

We thank D. Julius and F. Van Petegem for comments on the manuscript, J. Holton at ALS beamline 8.3.1 for data collection help, L.Y. Jan (University of California San Francisco) for the Kv4.3 clone and Minor laboratory members for support. This work was supported by awards to D.L.M. from the McKnight Foundation for Neuroscience, Rita Allen Foundation, Searle Scholars Award, Arnold and Mabel Beckman Foundation and US National Institutes of Health. G.L.H. was supported by US National Cancer Institute grant CA92584 and US Department of Energy contract DE-AC03-76SF00098. D.L.M. is a McKnight Scholar, Rita Allen Scholar, Searle Scholar and Beckman Young Investigator.

References

1. Hille, B. Ion Channels of Excitable Membranes. Sinauer Associates, Inc.; Sunderland, Massachusetts, USA: 2001.
2. Roux B. Ion conduction and selectivity in K(+) channels. Annu. Rev. Biophys. Biomol. Struct 2005;34:153–171. [PubMed: 15869387]
3. Tombola F, Pathak MM, Isacoff EY. How far will you go to sense voltage? Neuron 2005;48:719–725. [PubMed: 16337910]
4. Levitan IB. Signaling protein complexes associated with neuronal ion channels. Nat. Neurosci 2006;9:305–310. [PubMed: 16498425]
5. Rosati B, McKinnon D. Regulation of ion channel expression. Circ. Res 2004;94:874–883. [PubMed: 15087427]
6. Birnbaum SG, et al. Structure and function of Kv4-family transient potassium channels. Physiol. Rev 2004;84:803–833. [PubMed: 15269337]
7. Patel SP, Campbell DL. Transient outward potassium current, 'Ito', phenotypes in the mammalian left ventricle: underlying molecular, cellular and biophysical mechanisms. J. Physiol. (Lond.) 2005;569:7–39. [PubMed: 15831535]
8. An WF, et al. Modulation of A-type potassium channels by a family of calcium sensors. Nature 2000;403:553–556. [PubMed: 10676964]
9. Rhodes KJ, et al. KChIPs and Kv4 alpha subunits as integral components of A-type potassium channels in mammalian brain. J. Neurosci 2004;24:7903–7915. [PubMed: 15356203]
10. Guo W, Malin SA, Johns DC, Jeromin A, Nerbonne JM. Modulation of Kv4-encoded K(+) currents in the mammalian myocardium by neuronal calcium sensor-1. J. Biol. Chem 2002;277:26436–26443. [PubMed: 11994284]
11. Nakamura TY, et al. A role for frequenin, a Ca^{2+}-binding protein, as a regulator of Kv4 K^{+}-currents. Proc. Natl. Acad. Sci. USA 2001;98:12808–12813. [PubMed: 11606724]

12. Burgoyne RD, O'Callaghan DW, Hasdemir B, Haynes LP, Tepikin AV. Neuronal Ca^{2+}-sensor proteins: multitalented regulators of neuronal function. Trends Neurosci 2004;27:203–209. [PubMed: 15046879]
13. Bahring R, et al. Conserved Kv4 N-terminal domain critical for effects of Kv channel-interacting protein 2.2 on channel expression and gating. J. Biol. Chem 2001;276:23888–23894. [PubMed: 11287421]
14. Holmqvist MH, et al. Elimination of fast inactivation in Kv4 A-type potassium channels by an auxiliary subunit domain. Proc. Natl. Acad. Sci. USA 2002;99:1035–1040. [PubMed: 11805342]
15. Shibata R, et al. A fundamental role for KChIPs in determining the molecular properties and trafficking of Kv4.2 potassium channels. J. Biol. Chem 2003;278:36445–36454. [PubMed: 12829703]
16. Patel SP, Parai R, Parai R, Campbell DL. Regulation of Kv4.3 voltage-dependent gating kinetics by KChIP2 isoforms. J. Physiol. (Lond.) 2004;557:19–41. [PubMed: 14724186]
17. Scannevin RH, et al. Two N-terminal domains of Kv4 K(+) channels regulate binding to and modulation by KChIP1. Neuron 2004;41:587–598. [PubMed: 14980207]
18. Salvador-Recatala V, Gallin WJ, Abbruzzese J, Ruben PC, Spencer AN. A potassium channel (Kv4) cloned from the heart of the tunicate *Ciona intestinalis* and its modulation by a KChIP subunit. J. Exp. Biol 2006;209:731–747. [PubMed: 16449567]
19. Hatano N, Ohya S, Imaizumi Y. Functional interaction between KChIP1 and GFP-fused Kv4.3L co-expressed in HEK293 cells. Pflugers Arch 2002;444:80–88. [PubMed: 11976919]
20. Kuo HC, et al. A defect in the Kv channel-interacting protein 2 (KChIP2) gene leads to a complete loss of I(to) and confers susceptibility to ventricular tachycardia. Cell 2001;107:801–813. [PubMed: 11747815]
21. Long SB, Campbell EB, Mackinnon R. Crystal structure of a mammalian voltage-dependent Shaker family K+ channel. Science 2005;309:897–903. [PubMed: 16002581]
22. Kim LA, et al. Three-dimensional structure of I(to); Kv4.2-KChIP2 ion channels by electron microscopy at 21 Angstrom resolution. Neuron 2004;41:513–519. [PubMed: 14980201]
23. Zhou W, Qian Y, Kunjilwar K, Pfaffinger PJ, Choe S. Structural insights into the functional interaction of KChIP1 with Shal-type K(+) channels. Neuron 2004;41:573–586. [PubMed: 14980206]
24. Ren X, Shand SH, Takimoto K. Effective association of Kv channel-interacting proteins with Kv4 channel is mediated with their unique core peptide. J. Biol. Chem 2003;278:43564–43570. [PubMed: 12928444]
25. Derewenda ZS, Vekilov PG. Entropy and surface engineering in protein crystallization. Acta Crystallogr. D Biol. Crystallogr 2006;62:116–124. [PubMed: 16369101]
26. Kunjilwar K, Strang C, DeRubeis D, Pfaffinger PJ. KChIP3 rescues the functional expression of Shal channel tetramerization mutants. J. Biol. Chem 2004;279:54542–54551. [PubMed: 15485870]
27. Bourne Y, Dannenberg J, Pollmann V, Marchot P, Pongs O. Immunocytochemical localization and crystal structure of human frequenin (neuronal calcium sensor 1). J. Biol. Chem 2001;276:11949–11955. [PubMed: 11092894]
28. Callsen B, et al. Contribution of N- and C-terminal channel domains to Kv4.2 domains to KChIP interaction. J. Physiol. (Lond.) [corrected] 2005;568:397–412.
29. Svergun DI, Koch MHJ. Small-angle scattering studies of biological macromolecules in solution. Rep. Prog. Phys 2003;66:1735–1782.
30. Svergun DI. Determination of the regularization parameter in indirect-transform methods using perceptual criteria. J. Appl. Cryst 1992;25:495–503.
31. Svergun DI, Barberato C, Koch MHJ. CRYSOL—a program to evaluate X-ray solution scattering of biological macromolecules from atomic coordinates. J. Appl. Cryst 1995;28:768–773.
32. Svergun DI, Petoukhov MV, Koch MH. Determination of domain structure of proteins from X-ray solution scattering. Biophys. J 2001;80:2946–2953. [PubMed: 11371467]
33. Volkov VV, Svergun DI. Uniqueness of *ab initio* shape determination in small-angle scattering. J. Appl. Cryst 2003;36:860–864.

34. O'Callaghan DW, Hasdemir B, Leighton M, Burgoyne RD. Residues within the myristoylation motif determine intracellular targeting of the neuronal Ca^{2+} sensor protein KChIP1 to post-ER transport vesicles and traffic of Kv4 K+ channels. J. Cell Sci 2003;116:4833–4845. [PubMed: 14600268]
35. Minor DL Jr. et al. The polar T1 interface is linked to conformational changes that open the voltage-gated potassium channel. Cell 2000;102:657–670. [PubMed: 11007484]
36. Jerng HH, Covarrubias MK. + channel inactivation mediated by the concerted action of the cytoplasmic N- and C-terminal domains. Biophys. J 1997;72:163–174. [PubMed: 8994601]
37. Bahring R, Boland LM, Varghese A, Gebauer M, Pongs O. Kinetic analysis of open- and closed-state inactivation transitions in human Kv4.2 A-type potassium channels. J. Physiol. (Lond.) 2001;535:65–81. [PubMed: 11507158]
38. Gebauer M, et al. N-type inactivation features of Kv4.2 channel gating. Biophys. J 2004;86:210–223. [PubMed: 14695263]
39. Wang G, Covarrubias M. Voltage-dependent gating rearrangements in the intracellular T1–T1 interface of a K^+ channel. J. Gen. Physiol 2006;127:391–400. [PubMed: 16533897]
40. Wang G, et al. Functionally active t1-t1 interfaces revealed by the accessibility of intracellular thiolate groups in kv4 channels. J. Gen. Physiol 2005;126:55–69. [PubMed: 15955876]
41. Decher N, Barth AS, Gonzalez T, Steinmeyer K, Sanguinetti MC. Novel KChIP2 isoforms increase functional diversity of transient outward potassium currents. J. Physiol. (Lond.) 2004;557:761–772. [PubMed: 15107477]
42. Deschenes I, et al. Regulation of Kv4.3 current by KChIP2 splice variants: a component of native cardiac I(to)? Circulation 2002;106:423–429. [PubMed: 12135940]
43. Patel SP, Campbell DL, Morales MJ, Strauss HC. Heterogeneous expression of KChIP2 isoforms in the ferret heart. J. Physiol. (Lond.) 2002;539:649–656. [PubMed: 11897837]
44. Patel SP, Campbell DL, Strauss HC. Elucidating KChIP effects on Kv4.3 inactivation and recovery kinetics with a minimal KChIP2 isoform. J. Physiol. (Lond.) 2002;545:5–11. [PubMed: 12433945]
45. Bahring R, et al. Coupling of voltage-dependent potassium channel inactivation and oxidoreductase active site of Kvbeta subunits. J. Biol. Chem 2001;276:22923–22929. [PubMed: 11294861]
46. Rettig J, et al. Inactivation properties of voltage-gated K^+ channels altered by presence of beta-subunit. Nature 1994;369:289–294. [PubMed: 8183366]
47. Gu C, Jan YN, Jan LY. A conserved domain in axonal targeting of Kv1 (Shaker) voltage-gated potassium channels. Science 2003;301:646–649. [PubMed: 12893943]
48. Nakahira K, Shi G, Rhodes KJ, Trimmer JS. Selective interaction of voltage-gated K^+ channel beta-subunits with alpha-subunits. J. Biol. Chem 1996;271:7084–7089. [PubMed: 8636142]
49. Yang EK, Alvira MR, Levitan ES, Takimoto K. Kvbeta subunits increase expression of Kv4.3 channels by interacting with their C termini. J. Biol. Chem 2001;276:4839–4844. [PubMed: 11087728]
50. Deschenes I, Tomaselli GF. Modulation of Kv4.3 current by accessory subunits. FEBS Lett 2002;528:183–188. [PubMed: 12297301]
51. Hasdemir B, Fitzgerald DJ, Prior IA, Tepikin AV, Burgoyne RD. Traffic of Kv4 K^+ channels mediated by KChIP1 is via a novel post-ER vesicular pathway. J. Cell Biol 2005;171:459–469. [PubMed: 16260497]
52. Rosati B, et al. Concordant expression of KChIP2 mRNA, protein and transient outward current throughout the canine ventricle. J. Physiol. (Lond.) 2003;548:815–822. [PubMed: 12598586]
53. Rosati B, et al. Regulation of KChIP2 potassium channel beta subunit gene expression underlies the gradient of transient outward current in canine and human ventricle. J. Physiol. (Lond.) 2001;533:119–125. [PubMed: 11351020]
54. Kaab S, et al. Molecular basis of transient outward potassium current downregulation in human heart failure: a decrease in Kv4.3 mRNA correlates with a reduction in current density. Circulation 1998;98:1383–1393. [PubMed: 9760292]
55. Bowlby MR, et al. Identification and characterization of small molecule modulators of KChIP/Kv4 function. Bioorg. Med. Chem 2005;13:6112–6119. [PubMed: 16081294]

56. Van Petegem F, Clark KA, Chatelain FC, Minor DL Jr. Structure of a complex between a voltage-gated calcium channel beta-subunit and an alpha-subunit domain. Nature 2004;429:671–675. [PubMed: 15141227]

57. Kholod N, Mustelin T. Novel vectors for co-expression of two proteins in *E. coli*. Biotechniques 2001;31:322–3. 326–8. [PubMed: 11515368]

58. Minor DL Jr. Masseling SJ, Jan YN, Jan LY. Transmembrane structure of an inwardly rectifying potassium channel. Cell 1999;96:879–891. [PubMed: 10102275]

59. Nakamura TY, et al. Different effects of the Ca(2+)-binding protein, KChIP1, on two Kv4 subfamily members, Kv4.1 and Kv4.2. FEBS Lett 2001;499:205–209. [PubMed: 11423117]

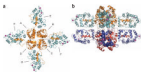

Figure 1.

Structure of the KChIP1–Kv4.3 T1 complex. (**a**) Overall structure of the complex as seen from the cytosolic side. KChIPs (cyan) and Kv4.3 components (orange) are shown as ribbons. Ca^{2+} (magenta spheres) and Zn^{2+} (black spheres) ions are also indicated. A–D and E–H label Kv4.3 and KChIP1 chains, respectively. Box marks the region shown in Figure 2d. (**b**) Side view of the two octameric complexes in the asymmetric unit, which are apposed on their cytoplasmic faces. Kv4.3 N-terminal domains (orange and red) and KChIP1s (cyan and slate blue) are shown. Dashed box marks the docking loop.

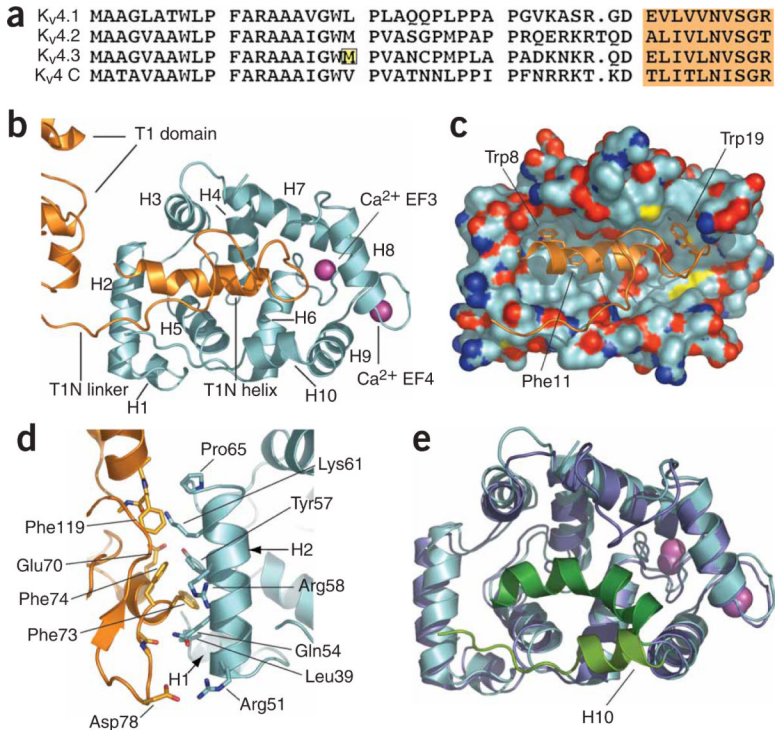

Figure 2.

Details of KChIP1–Kv4.3 T1N and T1 domain interactions. (**a**) Comparison of T1N regions from human (Kv4.1, Kv4.2 and Kv4.3) and tunicate (Kv4 C)[18] Kv4 channels. Orange indicates residues from the T1 domain. Rat and human Kv4.3 sequences are identical over the depicted region. Box indicates Kv4.3 T1N Met20. (**b**) Ribbon diagram of site 1 shows KChIP1 (cyan) and the Kv4.3 T1N helix, T1N linker and T1 domain (orange). KChIP1 helices H1–H10 are indicated. Ca^{2+} ions are shown as magenta spheres. (**c**) The three aromatic residues that anchor the T1N helix to KChIP1 are indicated as sticks (orange). The KChIP1 surface is shown with carbon (cyan), nitrogen (blue), oxygen (red) and sulfur (yellow) atoms indicated. (**d**) Ribbon diagram of site 2 interactions. Interface residues are shown as sticks and are labeled. (**e**) Superposition of KChIP1 from the KChIP1–$Kv4.3_{1–143}$ complex (cyan) and the KChIP1 monomer structure[17] (dark blue) reveals the conformational change in the H10 helix (green). The H10 helix from the KChIP1–$Kv4.3_{1–143}$ complex is indicated. The T1N helix is not shown. Calcium ions are shown as magenta spheres.

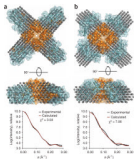

Figure 3.

SAXS analysis of the KChIP1–Kv4.3 T1 complex. (**a**) Top two images, superposition of the *ab initio* SAXS model with the X-ray structure of the KChIP1–Kv4.3 T1 domain structure. KChIPs are cyan and Kv4.3 N-terminal domain is orange. Bottom graph, comparison of the data and the calculated scattering curve from the X-ray structure ($\chi^2 = 3.03$). (**b**) Top two images, superposition of the *ab initio* SAXS model and a model in which the KChIPs orient along the T1 domain sides in a square, as suggested by EM microscopy[22]. Bottom chart, comparison of the data and the calculated scattering curve of the model ($\chi^2 = 7.06$). $s = (4\pi\sin(\theta))/\lambda$.

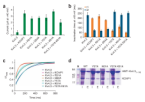

Figure 4.

Effects of site 2 mutations on KChIP1–Kv4.3 channel modulation and complex formation. (**a**) Peak currents at +40 mV for Kv4.3 alone and expressed with wild-type KChIP1 or indicated KChIP mutants. (**b**) Inactivation time constants at +40 mV for **a**. (**c**) Comparison of recovery from inactivation at +40 mV for **b**. In **a, b** and **c**, error bars show s.d. (**d**) MBP pull-down of $Kv4.3_{1–143}$, KChIP1 and KChIP mutants. I, column input; E, column eluate. Molecular weight markers (M; in kDa) are shown.

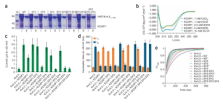

Figure 5.

Calcium effects on KChIP1–Kv4.3 complex formation and channel modulation. (**a**) MBP pull-down of $Kv4.3_{1–143}$, KChIP1 and KChIP mutants. I, column input; E, column eluate. Molecular weight markers (M; in kDa) are shown. (**b**) Circular dichroism of $KChIP1_{37–216}$ in the presence and absence of calcium (see key). All EGTA samples include 1 mM $CaCl_2$. (**c**) Peak currents at +40 mV for Kv4.3 alone and expressed with wild-type KChIP1 or indicated EF mutants. (**d**) Inactivation time constants at +40 mV for **c**. (**e**) Comparison of recovery from inactivation at +40 mV for **c**. In **c, d** and **e**, asterisks indicate data for a 3.5:1 Kv4.3/KChIP1 molar ratio. Error bars show s.d.

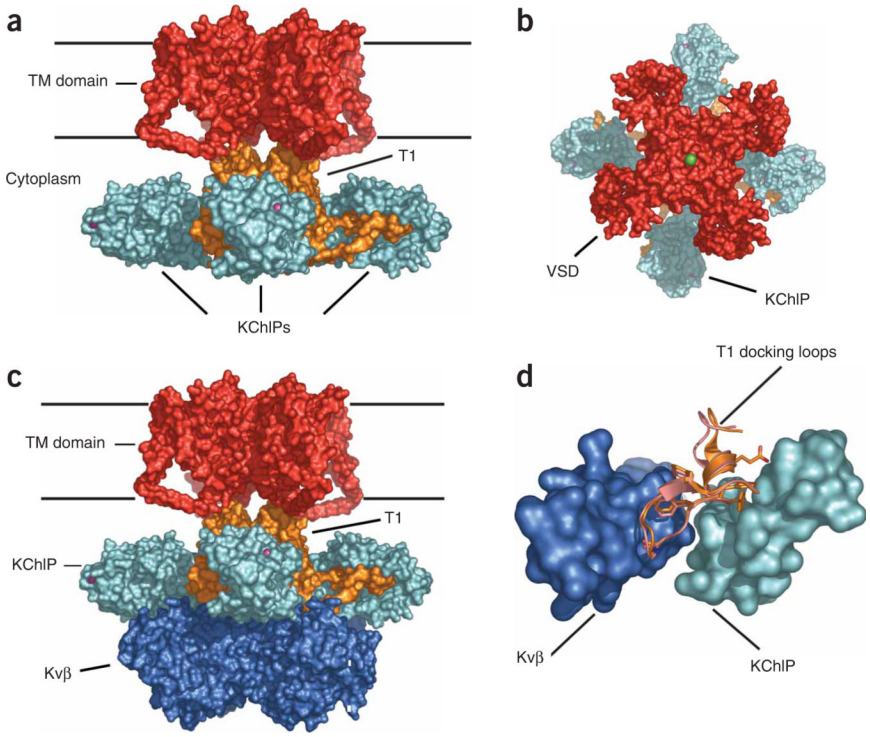

Figure 6.

Model of a Kv4.3–KChIP channel complex. (**a**) Model of the Kv4.3–KChIP complex based on the Kv1.2 structure[21]. KChIP1 (cyan), Kv4.3 T1 domain (orange) and the transmembrane domains (TM, dark red) are indicated. Calcium ions are magenta. Zinc ions are not visible. (**b**) View of model in **a** from the extracellular side. KChIP and voltage sensor domain (VSD) are indicated. Green sphere is a potassium ion in the pore. (**c**) Hypothetical model of a Kv4–KChIP–Kvβ complex. Domains are colored as in **a** with Kvβs indicated (dark blue). (**d**) Potential simultaneous engagement of the T1 docking loop by Kvβ and KChIP. Docking loop superposition for Kv1.2 (salmon) and Kv4.3 (orange) are shown. Surface shows the KChIP H1 and H2 helices (cyan) and the Kvβ interaction site (dark blue). Side chains for KChIP residues Glu40 and Lys50 and Kvβ residues Phe233 and His234 are omitted.

Table 1

Electrophysiology of Kv4.3–KChIP1 mutants

Test complexes	Current (μA)	Inactivation, τ_1 (ms)[a]	Inactivation, τ_2 (ms)[a]	Amplitude (%)[b]	Recovery, τ_{rec} (ms)[c]
Site 2 mutants					
Kv4.3 only	0.44 ± 0.27	44.65 ± 1.25	231.33 ± 28.32	75.14 ± 2.37	220.99 ± 52.14
Kv4.3 + KChIP1	3.42 ± 0.47	198.03 ± 6.8	71.76 ± 11.55	72.98 ± 3.49	52.57 ± 4.36
Kv4.3 + KChIP1 R51A	2.63 ± 0.3	219.73 ± 20.44	66.01 ± 9.34	69.55 ± 4.1	51.81 ± 3.96
Kv4.3 + KChIP1 Q54A	2.74 ± 0.25	179.58 ± 8.25	85.22 ± 8.66	76.55 ± 4.15	53.11 ± 2.13
Kv4.3 + KChIP1 Y57A	2.76 ± 0.48	68.18 ± 10.96	266.59 ± 18.25	65.84 ± 2.26	137.37 ± 20.39
Kv4.3 + KChIP1 K61A	3.75 ± 0.27	110.13 ± 18.84	234.06 ± 15.54	50.93 ± 2.12	110.19 ± 13.74
Kv4.3 + KChIP1 Y57A K61A	2.0 ± 0.5	48.6 ± 5.33	254.99 ± 18.69	71.03 ± 1.12	195.62 ± 33.92
EF-hand mutants					
Kv4.3 only	0.42 ± 0.14	39.03 ± 2.96	214.66 ± 8.06	72.36 ± 4.26	178.48 ± 14.06
Kv4.3 + KChIP1	3.45 ± 0.68	170.04 ± 4.77	50.33 ± 10.99	90.41 ± 3.51	49.29 ± 2.27
Kv4.3 + KChIP1[d]	1.83 ± 0.36	208.58 ± 8.58	50.08 ± 3.07	58.91 ± 3.84	72.47 ± 11.32
Kv4.3 + KChIP1 EF2	3.49 ± 0.75	173.27 ± 5.29	49.23 ± 13.3	88.54 ± 3.6	54.05 ± 6.52
Kv4.3 + KChIP1 EF3	3.25 ± 0.98	203.46 ± 10.35	54.67 ± 4.91	67.04 ± 5.4	58.14 ± 6.32
Kv4.3 + KChIP1 EF3[d]	0.68 ± 0.17	46.12 ± 2.52	240.19 ± 13.12	57.87 ± 1.76	99.31 ± 12.08
Kv4.3 + KChIP1 EF4	3.14 ± 0.61	184.31 ± 14.18	59.25 ± 18.48	71.62 ± 11.3	46.76 ± 3.94
Kv4.3 + KChIP1 EF2 EF3	2.11 ± 0.69	226.56 ± 8.12	46.25 ± 3.23	53.63 ± 2.2	90.85 ± 14.53
Kv4.3 + KChIP1 EF2 EF3[d]	0.39 ± 0.09	42.37 ± 3.63	235.87 ± 26.45	65.62 ± 5.12	144.01 ± 3.14
Kv4.3 + KChIP1 EF2 EF4	2.7 ± 0.61	195.69 ± 11.36	51.54 ± 7.23	65.5 ± 7.6	64.72 ± 12.51
Kv4.3 + KChIP1 EF3 EF4	0.54 ± 0.22	42.59 ± 0.95	248.39 ± 22.09	68.22 ± 8.5	120.62 ± 27.17
Kv4.3 + KChIP1 EF2 EF3 EF4	0.44 ± 0.16	36.68 ± 1.41	237.43 ± 35.45	68.71 ± 4.17	154.39 ± 30.97

All values were measured at +40 mV from a holding potential of –110 mV and represent means ± s.d. for five to eight oocytes.

[a] Inactivation time constants (τ_1 and τ_2) were obtained by fitting the inactivation time course to a sum of two exponentials.

[b] Amplitude indicates the relative contribution of the predominant inactivation component (τ_1).

[c] Recovery from inactivation (τ_{rec}) followed a single exponential function.

[d] Measurements made using 3.5:1 Kv4.3/KChIP1 mRNA.

Table 2

Data collection and refinement statistics

	Native	SeMet
Data collection		
Space group	*P*1	*P*1
Cell dimensions		
a, *b*, *c* (Å)	93.15, 98.11, 97.80	94.26, 98.36, 98.74
α, β, γ (°)	91.00, 112.96, 111.77	90.66, 112.96, 112.73
Resolution (Å)	50–3.35 (3.54–3.35)	50–4.20 (4.35–4.20)
R_{sym}	5.9 (42.5)	6.7 (48.3)
$I / \sigma I$	8.2 (1.7)	16.4 (1.6)
Completeness (%)	96.6 (96.9)	91.4 (70.1)
Redundancy	2.2 (2.2)	3.7 (3.3)
Refinement		
Resolution (Å)	50–3.35	
No. reflections	40,483	
R_{work} / R_{free}	23.7 / 26.8	
No. atoms		
Protein	18,965	
Ligand	28	
B-factors (Å^2)		
Protein	128.76	
Ligand/ion	132.92	
R.m.s. deviations		
Bond lengths (Å)	0.014	
Bond angles (°)	1.415	

One crystal was used for each data set. Values in parentheses are for highest-resolution shell.